Laser and Particle Beams (2012), *30*, 407–414.
© Cambridge University Press, 2012 0263-0346/12 $20.00
doi:10.1017/S0263034612000249

Time evolution of solid-density plasma during and after irradiation by a short, intense laser pulse

SHIXIA LUAN,[1] WEI YU,[1,2] MASAKATSU MURAKAMI,[2] HONGBIN ZHUO,[3] MINGYANG YU,[4,5] GUANGJIN MA,[1] AND KUNIOKI MIMA[2]

[1]Shanghai Institute of Optics and Fine Mechanics, Chinese Academy of Sciences, Shanghai, China
[2]Institute of Laser Engineering, Osaka University, Osaka 565-0871, Japan
[3]College of Science, National University of Defense Technology, Changsha, China
[4]Institute for Fusion Theory and Simulation, Zhejiang University, Hangzhou, China
[5]Institute for Theoretical Physics I, Ruhr University, Bochum, Germany

(Received 6 January 2012; Accepted 22 March 2012)

Abstract

A two-dimensional theoretical model for the evolution of solid-density plasma irradiated by short, intense laser pulse is introduced. The electrons near the target surface are pushed inward by the radiation pressure, leading to a receding electron density jump where the laser is reflected. The electrostatic field of the resulting charge separation eventually balances the radiation pressure at the laser peak. After that the charge separation field becomes dominant. It accelerates and compresses the ions that are left behind until they merge with the compressed electrons, resulting in a high-density plasma peak. The laser pulse reflected from the receding electron density jump loses energy in plasma and suffers Doppler frequency red-shift, which can provide valuable information on the laser absorption rate and the speed of the receding electrons. Electron oscillations, including the $\mathbf{u}\times\mathbf{B}$ oscillations across the density jump at twice the laser frequency during the laser action, as well as the low-frequency oscillations appearing after laser action, are identified.

Keywords: Electron density jump; Interaction of laser and solid plasma; Low-frequency oscillations; Theoretical model; $\mathbf{u}\times\mathbf{B}$ oscillations

1. INTRODUCTION

With advances in laser technology, pulses of very high intensity ($I_L\lambda_0^2 \geq 10^{20}$ Wcm$^{-2}\mu$m^2) and short (femtosecond) duration have become available (Perry & Mourou, 1994; Umstadter, 2003). Such ultrashort, ultraintense (USUI) laser pulses make possible exploration of intriguing phenomena related to laser interaction with solid-density plasmas, such as the acceleration of electrons and ions to high energies (Zhuo *et al.*, 2010; Yu *et al.*, 2010; Macchi *et al.*, 2005; Hatchett *et al.*, 2000; Koyama *et al.*, 2006; Limpouch *et al.*, 2008; Liu *et al.*, 2009; Malka & Fritzler, 2004; Mckenna *et al.*, 2008; Nickles *et al.*, 2007; Schwoerer *et al.*, 2006; Snavely *et al.*, 2000; Wang *et al.*, 2009; Yu *et al.*, 2005), generation of relativistic positrons (Chen *et al.*, 2009), production of intense quasi-static self-magnetic fields (Humphries & Petillo, 2000; Obenschain & Luhmann, 1979; Cai *et al.*, 2011), etc. These phenomena are not only important to basic physics but also pivotal to many novel applications such as laser-driven particle accelerators, ion lithography schemes (Alves *et al.*, 2006), hadron therapy (Bulanov & Khoroshkov, 2002; Salamin *et al.*, 2008), X-ray lasers (Tabak *et al.*, 1994), compact neutron sources (Disdier *et al.*, 1999), etc.

Because of the high nonlinearity involved, the interaction of USUI lasers with solid-density plasmas is traditionally investigated using particle-in-cell (PIC) numerical simulation. However, as pointed out by Berezhiani *et al.* (2005), multidimensional PIC simulation results are often difficult to interpret in terms of the basic underlying physics, since dimensional, kinetic, and other effects can mask and complicate the problem. To better visualize the basic interaction physics, it was proposed that the one-dimensional (1D) relativistic fluid-Maxwell equations be solved numerically. Indeed, Tushentsov *et al.* (2001) studied the evolution of the electrons and ions as a relativistic laser pulse penetrates overdense plasma with a 1D fluid-Maxwell code successfully. The Maxwell equations were solved under the slowly-varying-envelope paraxial approximation. Berezhiani *et al.* (2005) relaxed the latter approximation, but ignored the effects of ion motion.

Address correspondence and reprint requests to: Shixia Luan, 390 Qinghe Road, Jiading, Shanghai 201800, China. E-mail: sxluan@siom.ac.cn

https://doi.org/10.1017/S0263034612000249 Published online by Cambridge University Press

Theories of laser-plasma interaction usually start from the same equations as that of the fluid-Maxwell simulation. With suitable simplifications and standard derivation methods, relatively simple evolution equations are derived. In earlier theoretical works, valid for lasers of longer duration and lower intensity, the relativistic effect and ponderomotive effect are usually not included. Recently, 1D and two-dimensional (2D) relativistic theoretical models for the interactions of USUI lasers with solid-density plasmas have been developed (Yu *et al.*, 1998; Luan *et al.*, 2011), whose steady-state solutions describe short-time balance among the plasma electron response, the resulting charge separation fields, the ponderomotive force of the laser pulse, etc. The plasma ions are usually treated as immobile during the interaction.

Here we propose a 2D theoretical model for the time evolution of solid-density plasma *during* and *after* the irradiation by an USUI laser pulse normally incident on the solid-density plasma. Ion motion, which can become important after the laser action, is taken into account. Earlier theoretical works and computer simulations (Mishra *et al.*, 2009; Kemp *et al.*, 2008) on this topic consider lasers of semi-infinite duration, and the investigation is therefore confined to laser-plasma interaction. For USUI laser pulses, however, it is highly desirable to take into account the plasma behavior after laser action as well. In this model, we consider an axis-symmetric laser pulse of finite duration, such that the plasma evolution during and after the laser action can be investigated.

Section 2 contains a description of our theoretical model, which enables us to study the time-dependent behavior of laser and plasma. Section 3 focuses on the reflected laser pulse. With energy dissipation and frequency red-shift after interaction with the plasma, the reflected pulse can provide valuable information on laser absorption rate and electron recession speed. Section 4 considers the plasma response during and after laser action. As the laser pulse irradiates the solid target, the electrons near the target surface are pushed inward and piled up by the radiation pressure, leading to a receding electron density jump where the laser light is reflected. The positively charged massive ions respond to the laser action slowly and are left behind. The strong electrostatic field of charge separation balances with radiation pressure at the laser peak, which agrees well with the steady-state model proposed by Luan *et al.* (2011). After laser peak, the charge separation field becomes dominant. It accelerates and compresses the target ions. This process continues until the energetic ions join the laser-compressed electrons and results in a high-density plasma peak, which will keep moving inward inertially, even when the charge-separation field vanishes. Section 5 considers the electron oscillations across the compressed density jump. During laser action the $\mathbf{u}\times\mathbf{B}$ oscillation at twice laser frequency occurs for a linearly polarized laser. After laser action, a low-frequency electron oscillation is driven by the combined effect of space-charge field and electron inertia.

2. GOVERNING EQUATIONS

The starting equations for relativistic laser interaction with plasma can be written as (Luan *et al.*, 2011)

$$\partial_t \mathbf{p} = -\mathbf{E} - \nabla\gamma, \tag{1}$$

$$\partial_t \mathbf{p}_i = \mu\mathbf{E}, \tag{2}$$

$$\nabla\cdot\mathbf{E} = Zn_i - n, \tag{3}$$

$$\nabla\times(\nabla\times\mathbf{E}) + \partial_t^2\mathbf{E} = \partial_t(n\mathbf{u} - Zn_i\mathbf{u}_i), \tag{4}$$

where $\nabla\gamma = (\mathbf{u}\cdot\nabla)\mathbf{p} + \mathbf{u}\times\mathbf{B}$ is the ponderomotive force (Esarey *et al.*, 1996), $\mathbf{p} = \gamma\mathbf{u}$ and $\mathbf{p}_i = \gamma\mathbf{u}_i$ are the electron and ion momentum normalized by mc, $\mathbf{u}$ and $\mathbf{u}_i$ are the electron and ion velocities normalized by the speed of light c, γ and γ_i are the electron and ion relativistic factors, $-e$ and m are the electron charge and mass, n and n_i are the electron and ion densities normalized by the critical density n_c, Z is the ion charge number, $\mu = Zm/m_i$ and $\mathbf{E}$ is the electric field normalized by $mc\omega_0/e$. The time is normalized by ω_0^{-1} and the space coordinates by k_0^{-1} where ω_0 and k_0 are the laser frequency and wave number, respectively. The electron and ion continuity equations are

$$\partial_t n + \nabla\cdot(n\mathbf{u}) = 0, \tag{5}$$

$$\partial_t n_i + \nabla\cdot(n_i\mathbf{u}_i) = 0. \tag{6}$$

It is convenient to write the electric field as $\mathbf{E} = \mathbf{E}_t + \mathbf{E}_\ell$, where $\boldsymbol{E}_t = -\partial_t\mathbf{a}$ and $\mathbf{E}_\ell = -\nabla\phi$ are the transverse and longitudinal components satisfying $\nabla\cdot\mathbf{E}_t = 0$ and $\nabla\times\boldsymbol{E}_\ell = 0$, respectively, and the vector and scalar potentials $\mathbf{a}$ and ϕ have been normalized by mc^2/e. The two vector components can be used to describe the two modes appearing in plasma: the electromagnetic mode induced by laser penetration and the electrostatic (ES) mode induced by charge separation. Since the penetration depth is extremely small, one can assume that the vector potential $\mathbf{a}$ in the plasma remains in the same direction as that in the vacuum, i.e., perpendicular to the laser propagation direction. In fact, the overall laser penetration into the plasma is confined to a very small region on the order of the laser spot size in the transverse direction and the laser penetration depth in the axial, or propagation, direction. In solid-density plasma, the former is typically several tens laser wavelengths and the latter is far less than the laser wavelength. Accordingly, for electron momentum driven by laser fields we have $\mathbf{p}_t \approx \mathbf{p}_\perp = \mathbf{a}$, and the wave equation becomes

$$\nabla^2\mathbf{a} - \partial_t^2\mathbf{a} = (n/\gamma)\mathbf{a}. \tag{7}$$

In this way, we can treat the fast varying electron motion driven by electromagnetic mode without invoking the slowly varying envelope (parabolic) approximation.

The light pressure pushes the plasma electrons inward at target surface, forming a moving jump in the electron

https://doi.org/10.1017/S0263034612000249 Published online by Cambridge University Press

density. The massive ions can respond only slowly, so that an electrostatic field is induced by charge separation. Since the laser spot size is much larger than the penetration depth, the longitudinal field $\mathbf{E}_\ell$ evolves mainly in the axial direction, i.e., $\mathbf{E}_\ell \approx \mathbf{E}_{\ell z}$. The relativistic factor (Esarey *et al.*, 1996; Wang *et al.* 2009), is then given by

$$\gamma = \sqrt{1 + p_\perp^2 + p_z^2} = \sqrt{(1 + a^2)/(1 - u_z^2)}. \tag{8}$$

From Eqs. (1)–(3) we obtain for the ES components

$$\partial_t(\gamma u_z) = -E_z - \partial_z \gamma, \tag{9}$$

$$\partial_t(\gamma_i u_{iz}) = \mu E_z, \tag{10}$$

$$\partial_z E_z = Z n_i - n, \tag{11}$$

where for simplicity the subscript ℓ_z has been replaced by z. Eq. (11) can also be written as

$$\partial_t E_z = n u_z - Z n_i u_{iz}. \tag{12}$$

We write the incident laser pulse in vacuum in the form

$$\mathbf{E} = \mathbf{E}_s(\eta) X(\rho), \tag{13}$$

$$\mathbf{E}_s(\eta) = E_L \exp(-\eta^2/\tau^2)[\cos(\eta)\hat{x} + \sigma \sin(\eta)\hat{y}], \tag{14}$$

where $\eta = z - t$, $X(\rho) = \exp(-\rho^2/b^2)$ represents the radial profile of laser, $\rho = \sqrt{x^2 + y^2}$ is the radial coordinate, τ is the pulse duration, b is the spot size, $\sigma = 0$ and 1 denote linear and circular polarizations, respectively. Since the laser-plasma interaction region is extremely small, we can assume that the radial profile of the overall (both the transverse and longitudinal components) profile of the electric field in this region remains the same as that of the laser in vacuum. That is, the electric field in plasma can be expressed as $\mathbf{E} = \mathbf{E}_s(z, t)X(\rho)$, and we can write $\mathbf{a} = \mathbf{a}_s(z, t)X(\rho)$ and $E_z = E_{zs}(z, t)X(\rho)$, where a_s and E_{zs} are the amplitudes on the laser axis ($\rho \to 0$). One can then rewrite the wave equation (Eq. (7)) as

$$\partial_{zz} a_s - \partial_{tt} a_s - (4/b^2)a_s - (n_s/\gamma_s)a_s = 0. \tag{15}$$

For the ES parameters, we obtain from (9)–(12)

$$\partial_t(\gamma_s u_{zs}) = -E_{zs} - \partial_z \gamma_s, \tag{16}$$

$$\partial_t(\gamma_{is} u_{izs}) = \mu E_{zs}, \tag{17}$$

$$\partial_z E_{zs} = Z n_{is} - n_s, \tag{18}$$

$$\partial_t E_{zs} = n_s u_{zs} - Z n_{is} u_{izs}. \tag{19}$$

The continuity Eqs. (5) and (6) become

$$\partial_t n_s + \partial_z(n_s u_{zs}) = 0, \tag{20}$$

$$\partial_t n_{is} + \partial_z(n_{is} u_{izs}) = 0. \tag{21}$$

Eqs. (15)–(21) are solved using a second-order finite difference algorithm similar with the method used by Berezhiani *et al.* (2005). A grid is set up in both space coordinate z and time coordinate t. All physical quantities are defined on the grid nodes. The spatial step of the grid Δz is chosen to be 100 times shorter than the vacuum wavelength λ of the incident pulse. The temporal step Δt is dictated by the stability criterion of the scheme $c\Delta t/\Delta z < 1$. The wave equation was approximated by an implicit second-order discrete equation and solved by the modified Gauss method. For Eqs. (16)–(17) and (20)–(21), the first-order, explicit scheme was employed. To prevent density "overshooting," the Lax scheme was applied (Berezhiani *et al.*, 2005). Initial distribution of the laser field is localized in vacuum region sufficiently far from the solid plasma boundary. In this region, the scalar potential vanishes and the solution of Eq. (9) is $p_z = a_s^2/2$. The boundary conditions is $L(\pm\infty, t) = 0$, where $L \equiv (a_s, E_{zs}, p_z)$.

The above equations are solved to determine the laser and plasma parameters along the laser axis. From Eq. (11), we get for the density difference

$$\delta n = Z n_i - n = \delta n_s X(\rho). \tag{22}$$

The radial variations of the electron and ion densities are then given by

$$n = n(0) + [n_s - n(0)]X(\rho), \tag{23}$$

$$Z n_i = n(0) + [Z n_{is} - n(0)]X(\rho), \tag{24}$$

where $n(0) = Z n_i(0$ is the initial plasma density. Furthermore, for $\rho \gg b$, we have $n = Z n_i = n(0)$. With $a = a_s X(\rho)$, one can determine the radial profile of the vector potential, the relativistic factors, as well as the electron and ion velocities.

3. LASER DEPOSITION

We now consider the evolution of the laser pulse. Figure 1 shows the spatial profile of the vector potential at $t = 0$ and $30T_0$, where T_0 is the laser period, for normal incidence of a linearly polarized laser pulse on a semi-infinite overdense plasma. The initial plasma density is $n(0) = Z n_i(0) = 10$ for $z > 30$, and $n(0) = 0$ for $z < 30$. The incident laser strength is $a_L = 5$, the pulse duration is $\tau = 10T_0$, and the spot size is $b = 10\lambda$. At $t = 0$ the incident laser pulse is centered at $z = 15$. It propagates in vacuum to the right and interacts with the plasma at $z > 30$. At $t = 30T_0$ the laser pulse is reflected from the plasma and propagates again in vacuum to the left. As a result of the nonlinear interaction the reflected pulse is somewhat weaker and longer than the incident pulse.

Laser energy deposition in plasma is one of the key issues in laser plasma physics (Wilks *et al.*, 1992; Wilks & Kruer, 1997). The absorption rate can be defined as $f_{\text{abs}} = (W_{\text{in}} - W_{\text{out}})/W_{\text{in}}$, where W_{in} and W_{out} are the

https://doi.org/10.1017/S0263034612000249 Published online by Cambridge University Press

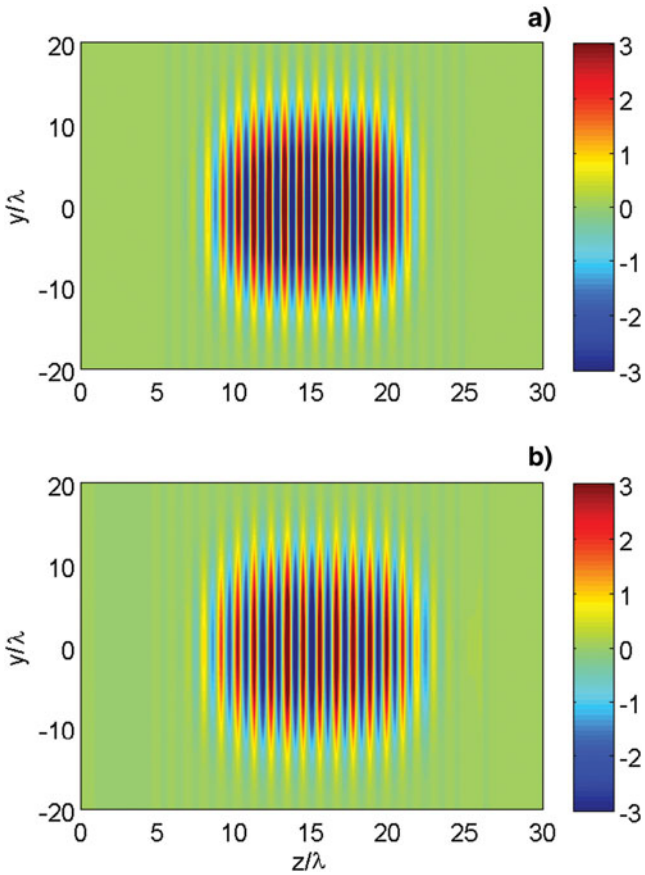


Fig. 1. (Color online) The laser amplitude a normalized by mc^2/e at (**a**) $t = 0$, and (**b**) $t = 30T_0$, for $a_L = 5$, $b = 10\lambda$, $\tau = 10T_0$, and $Zn_i = 10$.

energy of the incident and reflected laser pulses, respectively. Figure 2 shows the dependence of the absorption rate on the laser strength a_L, with the other parameters the same as in Figure 1. Our calculations show that the absorption rate first increases with the laser amplitude, reaches a maximum

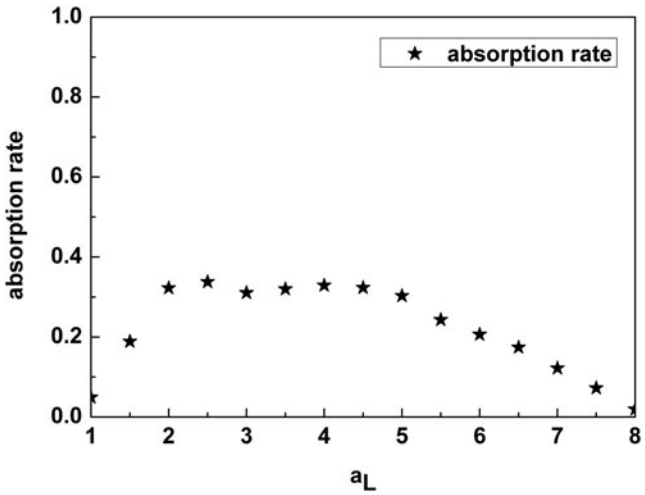


Fig. 2. The effect of initial laser intensity on laser absorption for $b = 10\lambda$, $\tau = 10T_0$, and $Zn_i = 10$.

(about 39%) at $a_L = 2.5$, and decreases as the amplitude further increases.

Valuable information can be obtained by analyzing the reflected radiation. Figure 3a shows the time evolution of the laser pulse along the laser axis at $z = 15$. The parameters of the interaction are the same as in Figure 1. Figure 3b shows the corresponding frequency spectrum, where the blue solid peak centered at $\omega/\omega_0 = 1$ is for the incident pulse, and the red dashed peak centered at $\omega/\omega_0 = 0.91$ is for the reflected pulse. The frequency of the reflected pulse is Doppler red-shifted since the laser pulse is reflected from a receding electron layer, acting like a moving mirror. From the Doppler frequency shift relation

$$\omega_r/\omega_i = (1 - v/c)/(1 + v/c), \tag{25}$$

where ω_r and ω_i are the frequencies of the reflected and incident light, we obtain a speed $v \sim 0.047c$ for the receding electron density jump.

4. PLASMA RESPONSE

We next examine the plasma response to the laser action. Figure 4 shows the 2D distributions of the (a) electron and

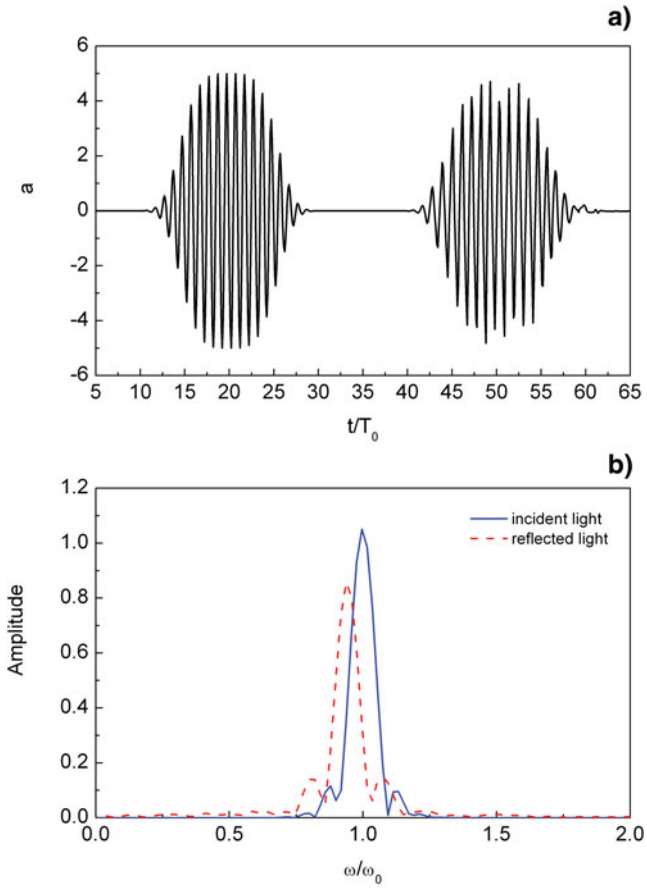


Fig. 3. (Color online) Time evolution (**a**) and frequency spectrum (**b**) of the incident (blue solid line) and reflected (red dashed line) laser pulses at $z = 15$. The parameters are the same as in Figure 1.

https://doi.org/10.1017/S0263034612000249 Published online by Cambridge University Press

(b) ion densities at $t = 14T_0$, when the laser interacts with plasma. The parameters are the same as for Figure 1. One can see from (a) that the radiation pressure, or the dc component of the ponderomotive force (Mishre *et al.*, 2009), pushes the electrons inward at the target surface and piles them up in front of the laser pulse, leading to a receding electron density jump. The density of the compressed electrons can be several times the initial target density. As shown in Figures 4b and 4c, the massive ions remain almost unmoved, so that an intense positive electrostatic charge-separation field E_z appears. The latter tends to accelerate the ions and decelerate the electrons. As the laser action continues, the charge separation field continues to increase until the peak of the laser pulse arrives at the compressed electron layer. A quasi-stationary state can then be established in the region, in which the space charge field balances the radiation pressure. Figure 4 shows the plasma response in such a state, which agrees well with that obtained from earlier steady-state modeling.

After the laser pulse is reflected and leaves the interaction region, the radiation pressure disappears and the space-charge field becomes dominant. It continues to accelerate the ions and decelerate the electrons. As time progresses the ion motion becomes more and more significant, so that the space-charge field becomes weaker and weaker. Figure 5 shows the distributions of the (a) electron density, (b) ion density, and (c) electrostatic field E_z at $t = 30T_0$. At the moment the former ion layer disappears, the ions there are accelerated by the space-charge field, until they join the electrons and move together inertially as a quasi-neutral fluid, as shown in Figures 5a and 5b. As a result, the space-charge field is greatly reduced. The resulting nearly-neutral high-density plasma peak continues to move forward inertially, even when the electrostatic field has vanished.

In the present model, collisions among the charged particles and plasma thermal effects are not included. During the time of laser interaction, these effects are safely negligible in the laser-driven short-timescale electron dynamics. However, in the later stages of the electron and ion evolution, collisions and thermal motion can be significant and even dominant. In particular, collisions can thermalize the dense plasma bunch, which will then expand as it propagates forward.

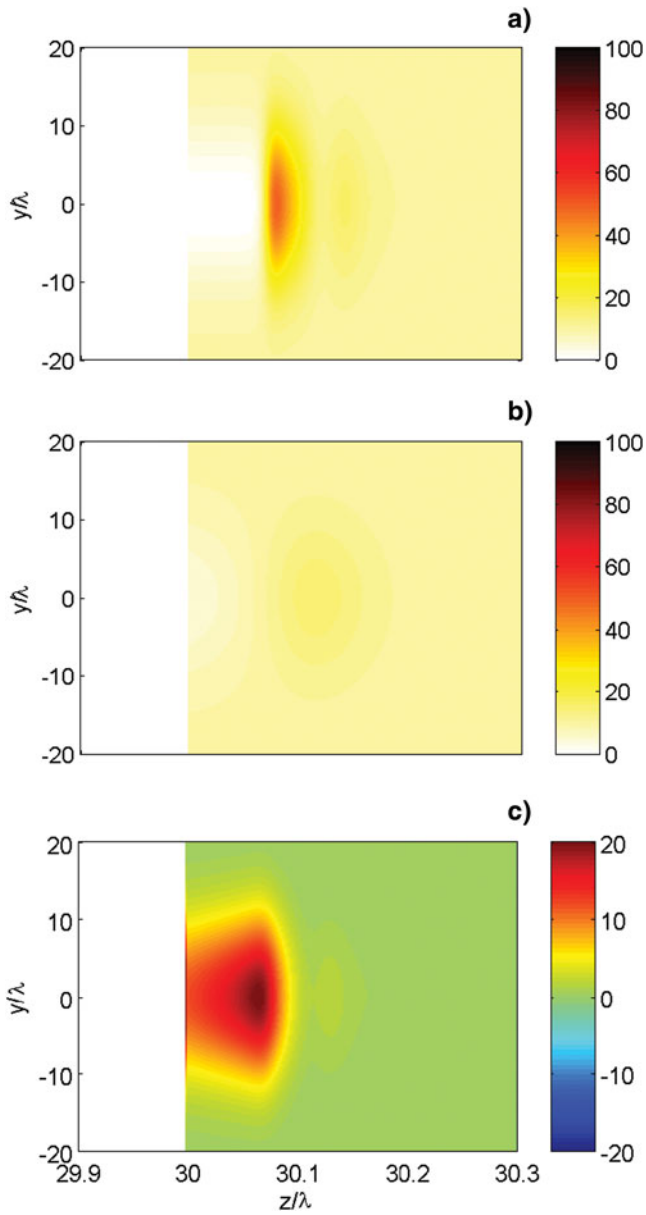


Fig. 4. (Color online) The electron density n (**a**), ion density n_i (**b**), normalized by the critical density n_c, and electrostatic charge-separation field (**c**) at $t = 14T_0$. The parameters are the same as in Figure 1.

5. ELECTRON OSCILLATIONS

Electron oscillation can appear across the density jump. Figure 6 shows the temporal and spatial profiles of the electron density along the laser axis, where the electron motion is strongest, for irradiation by (a) linearly and (b) circularly polarized laser pulses. The other parameters are the same as in Figure 1. In Figure 6a, one can see the receding electron density-jump (the red region). With $z_b(t)$ representing the position of density jump, the recession speed can be deduced from the density-jump trajectory $v = dz_b/dt \approx 0.046c$, which is in good agreement with that deduced from the Doppler frequency shift Eq. (25) and Figure 3b.

Two different types of electron oscillations can appear across the density jump. For the linearly polarized laser, $\mathbf{u} \times \mathbf{B}$ oscillation at twice the laser frequency (Luan *et al.*, 2011; Kruer & Estabrook, 1985) is dominant during ($t < 20T_0$) the laser action. Electrons near the density jump are pulled out twice a laser period and sent back by the oscillating component of the ponderomotive force, as shown in Figure 6a. Since the returning electrons have gained energy from the laser, they can easily propagate through the region of laser penetration and deposit their energy deep inside the target. This feature has invoked considerable research

https://doi.org/10.1017/S0263034612000249 Published online by Cambridge University Press

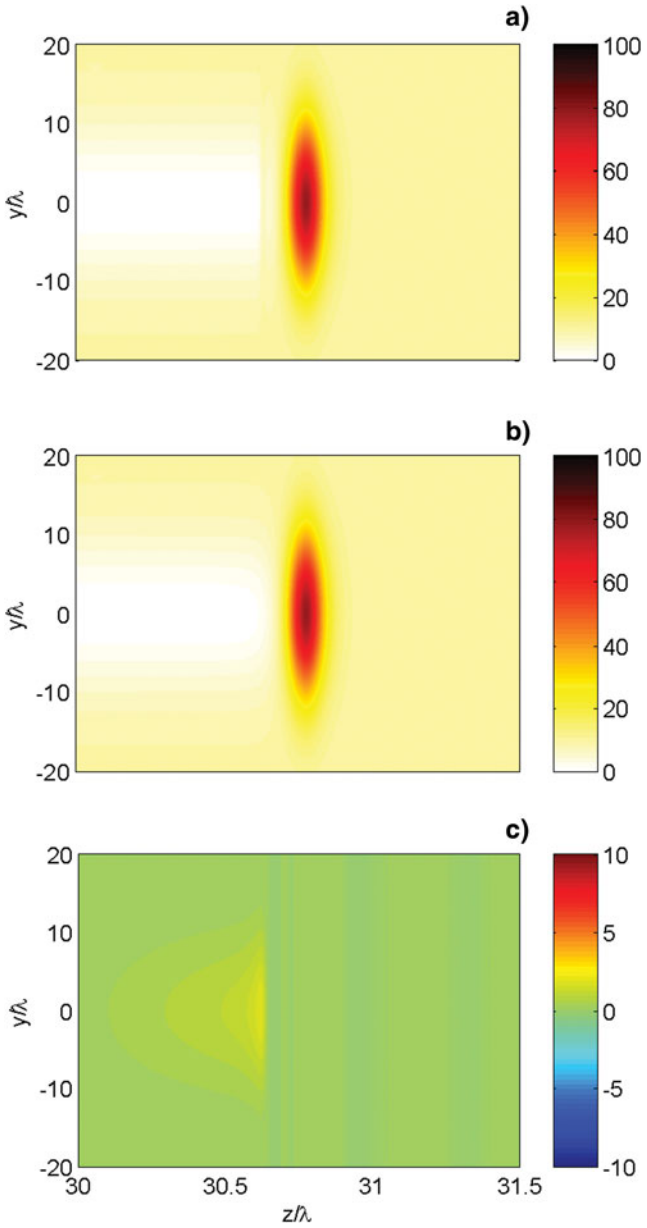


Fig. 5. (Color online) The electron density n (**a**), ion density n_i (**b**), normalized by the critical density n_c, and electrostatic charge-separation field (**c**) at $t = 30T_0$. The parameters are the same as in Figure 1.

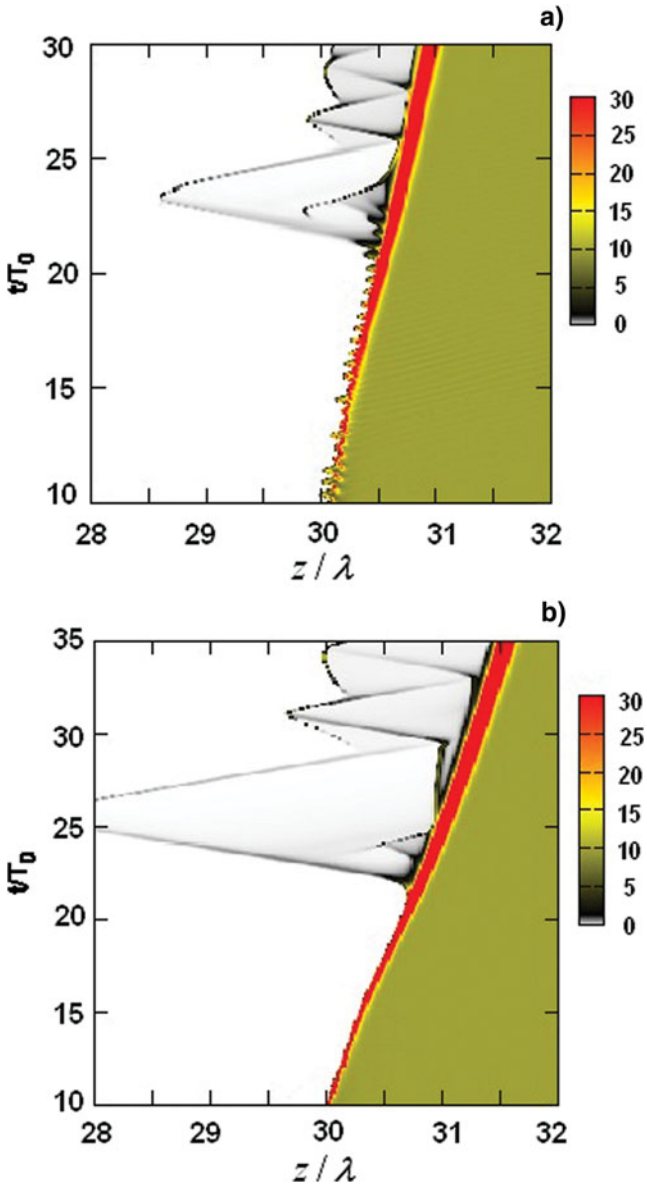


Fig. 6. (Color online) Evolution of the electron density along the laser axis for linearly (**a**) and circularly (**b**) polarized laser pulses for $a_L = 5$, $b = 10\lambda$, $\tau = 10T_0$, and $Zn_i = 10$. In (a) one can clearly see the $\mathbf{u} \times \mathbf{B}$ oscillations at the layer surface. Very low frequency and density space charge oscillations appear for both cases after the laser action.

interest and should be useful for fast ignition in inertial confined fusion. For a circularly polarized laser pulse, however, the $\mathbf{u} \times \mathbf{B}$ oscillations do not occur during the laser action, as shown in Figure 6b for $t < 20T_0$. On the other hand, it is found that for both linearly and circularly polarized lasers, low-frequency-low-density electron bunch oscillations can occur at the layer surface after the laser action has ended. As mentioned, at the initial stage of the interaction, the radiation pressure pushes plasma electrons inward and establishes a strong space-charge field. After the laser peak, the space-charge field becomes dominant and pulls the electrons backward. These electrons will not stop at the target surface (their initial position before laser action). Instead, they will keep moving outward inertially. A space-charge field pointing the opposite direction is thus established, and decelerates the outgoing electrons and then accelerates them inward. Such an action can start a lower (compared to the laser frequency) frequency space-charge oscillation with decreasing period and amplitude, as shown in Figure 6 for $t > 20T_0$. Figure 6 also shows that with the circularly polarized laser the post-pulse electron oscillations are more intense. This can be expected, since for the same $a_L$the ponderomotive force of a circularly polarized laser is stronger than that of a linearly polarized one, so that a stronger space charge field is established. For the same reason, the forward speed

https://doi.org/10.1017/S0263034612000249 Published online by Cambridge University Press

of the compressed layer is also higher for the circularly polarized laser, as can be seen in Figure 6.

6. SUMMARY

In this paper, a 2D theoretical model of the evolution of solid-density plasma *during* and *after* irradiation by a normally incident USUI laser pulse is proposed. As the laser pulse irradiates the target, the electrons at the surface are pushed inward by radiation pressure while the massive ions are left behind, leading to a receding electron density jump and a positively charged ion layer. As the peak radiation intensity interacts with the compressed electron layer, the strong electrostatic charge separation field is balanced by the radiation pressure, and a quasi-stationary state is established. After the laser light reflects, the charge separation field accelerates and compresses the ions in the region and decelerates the inertially forward propagating electron layer until the energetic ions merge with the compressed electrons. The resulting high-density neutral plasma peak will keep propagating forward inertially, even after the charge-separation field vanishes. During the interaction the laser pulse loses energy in the plasma and is reflected. The reflected pulse is frequency red-shifted because of the receding electron layer. The laser energy absorption rate and the speed of the electron layer are obtained. Moreover for a linearly polarized laser, during the laser action $\mathbf{u} \times \mathbf{B}$ oscillations at twice laser frequency appear on the surface of the electron layer. For both linearly and circularly polarized lasers, low-frequency oscillations appear after laser action due to the joint effect of space-charge field and electron inertia. In future work we intend to extend our model to thin foil targets and to study the mechanisms of doubly charged ion acceleration (Yu *et al.*, 2010).

ACKNOWLEDGMENTS

This work was supported by the Natural Science Foundation of China under Grant Nos. 11174303, 10975185, 11175253; the Science and Technology Commission of Shanghai Municipality under Grant No. 08PJ14102, the 973 Program under Grant Nos. 2008CB717806 and 2011CB808104, and the Ministry of Science and Technology of China ITER Project under Grant No. 2009GB105005.

REFERENCES

Alves, A., Reichart, P., Siegele, R., Johnston, P.N. & Jamieson, D.N. (2006). Ion beam ithography using single ions. *Nucl. Instrum. Meth. Phys. Res. B* **249**, 730–733.

Bulanov, S.V. & Khoroshkov, V.S. (2002). Feasibility of using laser ion accelerators in Proton therapy. *Plasma Phys. Rep*. **28**, 453–456;

Berezhiani, V.I., Garuchava, D.P., Mikeladze, S.V., Sigua, K.I., Tsintsadze, N.L., Mahajan, S.M., Kishimoto, Y. & Nishikawa, K. (2005). Fluid-Maxwell simulation of laser pulse dynamics in overdense plasma. *Phys. Plasmas* **12**, 062308.

Cai, H.B., Zhu, S.P., Chen, M., Wu, S.Z., He, X.T. & Mima, K. (2011). Magnetic-field generation and electron-collimation analysis for propagating fast electron beams in overdense plasmas. *Phys. Rev. E* **83**, 036408.

Chen, H., Wilks, S.C., Bonlie, J.D., Liang, E.P., Myatt, J., Price, D.F., Meyerhofer, D.D. & Beiersdorfer, P. (2009). Relativistic positron creation using ultraintense short pulse lasers. *Phys. Rev. Lett*. **102**, 105001.

Disdier, L., Garçonnet, J.P., Malka, G. & Miquel, J.L. (1999). Fast neutron emission from a high-energy ion beam produced by a high-intensity subpicosecond laser pulse. *Phys. Rev. Lett*. **82**, 1454–1457.

Esarey, E., Sprangle, P., Krall, J. & Ting, A. (1996). Overview of plasma-based accelerator concepts. *IEEE Trans. Plasma Sci*. **24**, 252–288.

Hatchett, S.P., Brown, C.G., Cowan, T.E., Henry, E.A., Johnson, J.S., Key, M.H., Koch, J.A., Langdon, A.B., Lasinski, B.F., Lee, R.W., Mackinnon, A.J., Pennington, D.M., Perry, M.D., Phillips, T.W., Roth, M., Sangster, T.C., Singh, M.S., Snavely, R.A., Stoyer, M.A., Wilks, S.C. & Yasuike, K. (2000). Electron, photon, and ion beams from the relativistic interaction of petawatt laser pulses with solid targets. *Phys. Plasmas* **7**, 2076–2082.

Humphries, S. & Petillo, J. (2000). Self-magnetic field calculations in ray-tracing codes. *Laser Part. Beams* **18**, 601–610.

Kemp, A.J., Sentoku, Y. & Tabak, M. (2008). Hot-electron energy coupling in ultraintense laser-matter interaction. *Phys. Rev. Lett*. **101**, 075004.

Koyama, K., Adachi, M., Miura, E., Kato, S., Masuda, S., Watanabe, T., Ogata, A. & Tanimoto, M. (2006). Monoenergetic electron beam generation from a laser-plasma accelerator. *Laser Part. Beams* **24**, 95–100.

Kruer, W.L. & Estabrook, K. (1985). $\mathbf{J} \times \mathbf{B}$ heating by very intense laser light. *Phys. Fluids B* **28**, 430–432.

Limpouch, J., Psikal, J., Andreev, A.A., Platonov, K.Y. & Kawata, S. (2008). Enhanced laser ion acceleration from mass-limited targets. *Laser Part. Beams* **26**, 225–534.

Liu, M.P., Xie, B.S., Huang, Y.S., Liu, J. & Yu, M.Y. (2009). Enhanced ion acceleration by collisionless electrostatic shock in thin foils irradiated by ultraintense laser pulse. *Laser Part. Beams* **27**, 327–333.

Luan, S.X., Yu, W., Yu, M.Y., Ma, G.J., Zhang, Q.J., Sheng, Z.M. & Murakami, M. (2011). Analytical model for interaction of short intense laser pulse with solid target. *Phys. Plasmas* **18**, 042701.

Macchi, A., Cattani, F., Liseykina, T.V. & Cornolti, F. (2005). Laser acceleration of ion bunches at the front surface of overdense plasmas. *Phys. Rev. Lett*. **94**, 165003.

Malka, V. & Fritzler, S. (2004). Electron and proton beams produced by ultra short laser pulses in the relativistic regime. *Laser Part. Beams* **22**, 399–405.

Mckenna, P., Carroll, D.C., Lundh, O., Nurnberg, F., Markey, K., Bandyopadhyay, S., Batani, D., Evans, R.G., Jafer, R., Kar, S., Neely, D., Pepler, D., Quinn, M.N., Redaelli, R., Roth, M., Wahlstrom, C.G., Yuan, X.H. & Zepf, M. (2008). Effects of front surface plasma expansion on proton acceleration in ultraintense laser irradiation of foil targets. *Laser Part. Beams* **26**, 591–596.

Mishra, R., Sentoku, Y. & Kemp, A.J. (2009). Hot electron generation forming a steep interface in superintense laser-matter interaction. *Phys. Plasmas* **16**, 112704.

https://doi.org/10.1017/S0263034612000249 Published online by Cambridge University Press

Nickles, P.V., Ter-Avetisyan, S., Schnuerer, M., Sokollik, T., Sandner, W., Schreiber, J., Hilscher, D., Jahnke, U., Andreev A. & Tikhonchuk, V. (2007). Review of ultrafast ion acceleration experiments in laser plasma at Max Born Institute. *Laser Part. Beams* **25**, 347–363.

Obenschain, S.P. & Luhmann, N.C. (1979). Self-magnetic-field generation in a plasma. *Phys. Rev. Lett*. **42**, 311–314.

Perry, M.D. & Mourou, G. (1994). Terawatt to petawatt subpicosecond Lasers. *Sci*. **264**, 917–924.

Salamin, Y.I., Harman, Z. & Keitel, C.H. (2008). Direct high-power laser acceleration of ions for medical applications. *Phys. Rev. Lett*. **100**, 155004.

Schwoerer, H., Pfotenhauer, S., Jackel, O., Amthor, K.-U., Liesfeld, B., Ziegler, W., Sauerbrey, R., Ledingham, K.W.D. & Esirkepov, T. (2006). Laser-plasma acceleration of quasimonoenergetic protons from microstructured targets. *Nat*. **439**, 445–448.

Snavely, R.A., Key, M.H., Hatchett, S.P., Cowan, T.E., Roth, M., Phillips, T.W., Stoyer, M.A., Henry, E.A., Sangster, T.C., Singh, M.S., Wilks, S.C., Mackinnon, A., Offenberger, A., Pennington, D.M., Yasuike, K., Langdon, A.B., Lasinski, B.F., Johnson, J., Perry, M.D. & Campbell, E.M. (2000). Intense high-energy proton beams from petawatt-laser irradiation of solids. *Phys. Rev. Lett*. **85**, 2945–2948.

Tabak, M., Hammer, J., Glinsky, M.E., Kruer, W.L., Wilks, S.C. Woodworth, J., Campbell, E.M., Perry, M.D. & Mason, R.J. (1994). Ignition and high gain with ultrapowerful lasers. *Phys. Plasmas* **1**, 1626–1634.

Tushentsov, M., Kim, A., Cattani, F., Anderson, D. & Lisak, M. (2001). Electromagnetic energy penetration in the self-induced transparency regime of relativistic laser-plasma interactions. *Phys. Rev. Lett*. **87**, 275002.

Umstadter, D. (2003). Relativistic laser–plasma interactions. *J. Phys. D* **36**, 151–165.

Wang, X., Yu, W., Yu, M.Y., Senecha, V.K., Xu, H., Wang, J.W., Yuan, X. & Sheng, Z.M. (2009). Efficient acceleration of a small dense plasma pellet by consecutive action of multiple short intense laser pulses. *Laser Part. Beams* **27**, 629–634.

Wang, X., Yu, W., Yu, M.Y., Xu, H., Wang, J.W. & Yuan, X. (2009). Simple model for wakefield excitation by intense short-pulse laser in underdense plasma. *Phys. Plasmas* **16**, 053107.

Wilks, S.C. & Kruer, W.L. (1997). Absorption of ultrashort, ultra-intense laser light by solids and overdense plasmas. *IEEE J. Quan. Elect*. **33**, 1954–1968.

Wilks, S.C., Kruer, W.L., Tabak, M. & Langdon, A.B. (1992). Absorption of ultra-intense laser pulses. *Phys. Rev. Lett*. **69**, 1383–1386.

Yu, T.P., Pukhov, A., Shvets, G. & Chen, M. (2010). Simulations of stable compact proton beam acceleration from a two-ion-species ultrathin foil. *Phys. Rev. Lett*. **105**, 065002.

Yu, W., Xu, H., He, F., Yu, M.Y., Ishiguro, S., Zhang, J. & Wong, A.Y. (2005). Direct acceleration of solid-density plasma bunch by ultraintense laser. *Phys. Rev. E* **72**, 046401.

Yu, W., Yu, M.Y., Sheng, Z.M. & Zhang, J. (1998). Model for fast electrons in ultrashort-pulse laser interaction with solid targets. *Phys. Rev. E* **58**, 2456–2460.

Zhuo, H.B., Chen, Z.L, Yu, Wei., Sheng, Z.M., Yu, M.Y., Jin, Z. & Kodama, R. (2010). Quasimonoenergetic proton bunch generation by dual-peaked electrostatic-field acceleration in foils irradiated by an intense linearly polarized laser. *Phys. Rev. Lett*. **105**, 065003.

https://doi.org/10.1017/S0263034612000249 Published online by Cambridge University Press